

HERMITIAN APPROXIMATION OF THE SPHERICAL DIVERGENCE ON THE CUBED-SPHERE

JEAN-PIERRE CROISILLE †‡

ABSTRACT. Previous work [7] showed that the Cubed-Sphere grid offers a suitable discrete framework for extending Hermitian compact operators [6] to the spherical setup. In this paper we further investigate the design of high-order accurate approximations of spherical differential operators on the Cubed-Sphere with an emphasis on the spherical divergence of a tangent vector field. The basic principle of this approximation relies on evaluating pointwise Hermitian derivatives along a series of great circles covering the sphere. Several test-cases demonstrate the very good accuracy of the approximate spherical divergence calculated with the new scheme.

Keywords: Cubed-Sphere grid - spherical divergence - spherical laplacian - finite difference scheme - Hermitian compact operator - Spherical Harmonics.

1. INTRODUCTION

Recently accurate approximations of partial differential equations on the sphere have become increasingly demanded. Many fields in physics beyond Global Climatology Modeling, where calculations on the rotating earth is a core practice, now require a significant use of the spherical context. These include

- *Medical imaging:* The inverse Radon transform consists in approximating spectral data on the sphere in a fast and accurate manner [20].
- *Gravitational field analysis:* Specialized satellite data (from the COBE satellite) must be thoroughly worked out by interpolation and approximation [14].
- *Celestial data analysis:* Data given on the celestial sphere also require an accurate treatment [25].

In this work the principle behind approximating spherical differential operators [7] is further applied to the spherical divergence. Our compact approximation is performed on The Cubed-Sphere [16, 5, 11]. It uses a methodology based on the following steps [7]:

- Interpolation of data on a series of great circles using the fact that coordinate lines are great circles sections.
- Calculation of Hermitian finite-difference derivatives along these great circles. This step is purely one-dimensional and periodic, only requiring tridiagonal (periodic) linear systems to be solved.
- Reconstruction of spherical differential operator on each panel of the Cubed-Sphere using a suitable change of variables.

The expected fourth-order accuracy inherited from Hermitian approximations was observed. This is particularly important for calculations where second order accuracy is not sufficient. It is the case for example for calculating complex fluid flow patterns, such as turbulent flows, or quasi incompressible

Date: November 29, 2014.

This work was made during a sabbatical year at the C.N.R.S. (Centre National de la Recherche Scientifique, France). The author thanks N. Paldor for his support and encouragement. This work also benefited from helpful discussions with M. Ben-Artzi, F. Bouchut and T. Dubos.

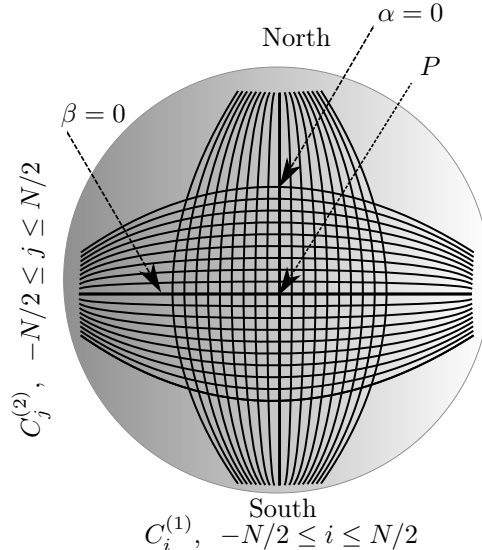


FIGURE 1. The points of the Cubed Sphere are obtained as intersections of two families of great circles. The circles in *vertical* (South-North) position are labeled $C_i^{(1)}$, $-N/2 \leq i \leq N/2$. The circles in *horizontal* (East-West) position are labeled $C_j^{(2)}$, $-N/2 \leq j \leq N/2$. The isovalues circles $\alpha = 0$ and $\beta = 0$ are indicated. The point P serves as the center of each family of great circles.

flows. Other important examples can be found in Global Climatology Modeling, where several series of test-cases have been suggested [21, 13, 12]. These tests offer an excellent platform for assessing the efficiency of numerical schemes for PDE's approximations on the sphere.

The outline of the paper is as follows. In Section 2 the fundamental principle for Hermitian approximation is recalled. In Section 3 the calculation of the spherical gradient [7] is recalled. Section 4 is devoted to calculating the spherical divergence of a tangential vector field. In Section 5 several results showing numerical evidence of the fourth-order accuracy are presented. After the conclusion (Section 6), standard geometric notation used throughout the paper is recalled in Section 7.

2. THE CUBED-SPHERE GRID

2.1. Panels and geodesic coordinate lines. In this section we present the Cubed-Sphere grid described in [23]. This grid is commonly used for simulation of the dynamics of the atmosphere. Refer to [28, 18] and the references therein. In the sequel we emphasize why this grid is well adapted to calculate high order discrete differential operators in the Hermitian fashion. Note moreover that all our calculations are done on the sphere itself and not on the faces of the cube in which the sphere is embedded.

The design of the Cubed-Sphere is based on great circles, i.e. geodesic lines of the sphere \mathbb{S}^2 equipped with the standard metric. Consider the two sets of great circles called $C_i^{(1)}$ and $C_j^{(2)}$ shown in Fig.1. These two sets are constructed as follows. The set $C_i^{(1)}$ consists of a collection of great circles in *South-North* (meridional) position, passing through the South and North poles. A point P is selected on one of these great circles and will serve as the center of the grid described in what follows.

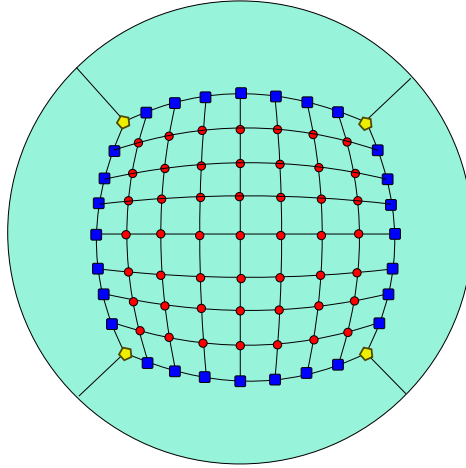


FIGURE 2. The points of a typical panel of the Cubed-Sphere are classified in three categories: (i) Circles correspond to *internal* points; (ii) Squares correspond to *edge* points ; (iii) Pentagons correspond to *corner* points

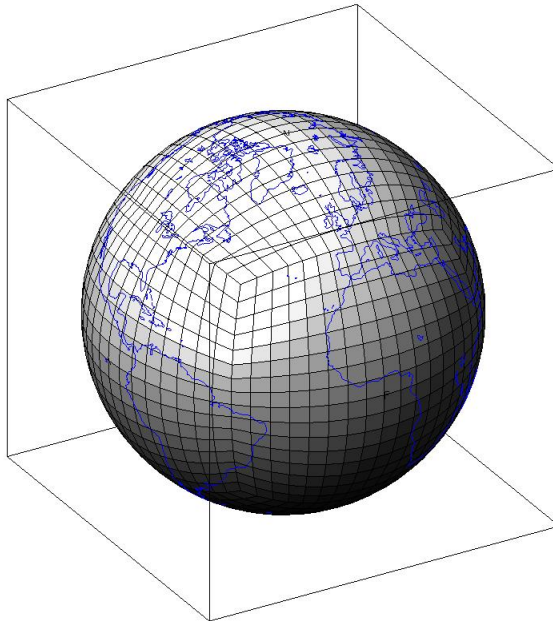


FIGURE 3. The Cubed-Sphere grid with a grid parameter of $N = 16$. The total number of points is $6 \times 16^2 + 2 = 1538$ in this case.

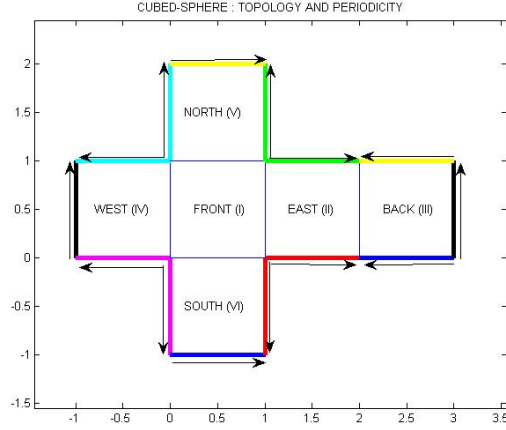


FIGURE 4. Topology and spherical periodicity of the six panels of the Cubed-Sphere. The Latin numbers (I), (II), (III), (IV), (V) and (VI) designate the panels *Front*, *East*, *Back*, *West*, *North* and *South*.

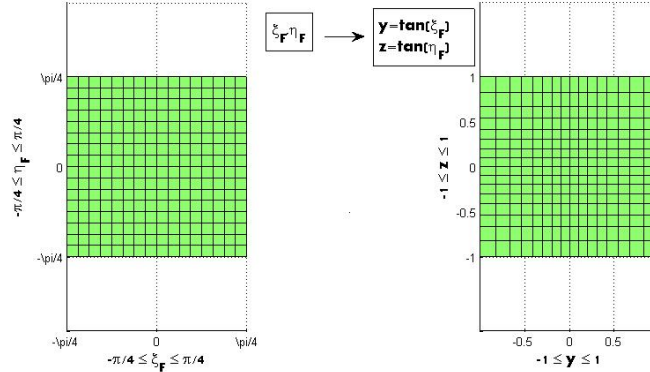


FIGURE 5. The grid of Panel (I) in both (ξ, η) coordinates and in physical coordinates. Left: regular Cartesian grid with coordinates (ξ, η) . Right: $x = 1$ cube face with *gnomonic coordinates* $(Y, Z) = (\tan(\xi), \tan(\eta))$.

Let the set $C^{(1)}$ rotate by 90° around P : one obtains a second set of circles called $C_j^{(2)}$. The circles $C_j^{(2)}$ are orthogonal to the circle labeled $C_0^{(1)}$ (see Fig. 1). The points $\mathbf{s}_{i,j} = C_i^{(1)} \cap C_j^{(2)}$ form a spherical section centered at P . Such a section will be called a *panel*.

Along each circle $C_j^{(2)}$ the geodesic angle with origin along $C_0^{(1)}$ is called α . Similarly the geodesic angle along each circle $C_i^{(1)}$ with origin along $C_0^{(2)}$ is called β . A canonical tangent vector basis at point $\mathbf{s}_{i,j}$ is $(\mathbf{e}_\alpha(\mathbf{s}_{i,j}), \mathbf{e}_\beta(\mathbf{s}_{i,j}))$ where $\mathbf{e}_\alpha(\mathbf{s}_{i,j})$, (resp. $\mathbf{e}_\beta(\mathbf{s}_{i,j})$) is the tangent unit vector to the circle $C_j^{(2)}$ (resp. $C_i^{(1)}$) at $\mathbf{s}_{i,j}$. The basis $(\mathbf{e}_\alpha(\mathbf{s}_{i,j}), \mathbf{e}_\beta(\mathbf{s}_{i,j}))$ is in general non-orthogonal, unless $\mathbf{s}_{i,j}$ is located on the circles $\alpha = 0$ or $\beta = 0$, see Fig. 1.

Let $(\mathbf{e}^\alpha(\mathbf{s}_{i,j}), \mathbf{e}^\beta(\mathbf{s}_{i,j}))$ be the dual basis defined by the relations

$$(1) \quad \begin{cases} \mathbf{e}^\alpha(\mathbf{s}_{i,j}) \cdot \mathbf{e}_\alpha(\mathbf{s}_{i,j}) = 1, \\ \mathbf{e}^\alpha(\mathbf{s}_{i,j}) \cdot \mathbf{e}_\beta(\mathbf{s}_{i,j}) = 0, \end{cases} \quad \text{and} \quad \begin{cases} \mathbf{e}^\beta(\mathbf{s}_{i,j}) \cdot \mathbf{e}_\alpha(\mathbf{s}_{i,j}) = 0, \\ \mathbf{e}^\beta(\mathbf{s}_{i,j}) \cdot \mathbf{e}_\beta(\mathbf{s}_{i,j}) = 1. \end{cases}$$

For any regular function $\mathbf{s} \in \mathbb{S}^2 \mapsto u(\mathbf{s})$, let $\nabla_T u(\mathbf{s})$ be the tangential gradient. It is expressed at $\mathbf{s}_{i,j}$ by

$$(2) \quad \nabla_T u(\mathbf{s}_{i,j}) = \frac{\partial u}{\partial \alpha}(\mathbf{s}_{i,j}) \mathbf{e}^\alpha(\mathbf{s}_{i,j}) + \frac{\partial u}{\partial \beta}(\mathbf{s}_{i,j}) \mathbf{e}^\beta(\mathbf{s}_{i,j}).$$

In (2) the partial derivatives $\frac{\partial u}{\partial \alpha}(\mathbf{s}_{i,j})$ (resp. $\frac{\partial u}{\partial \beta}(\mathbf{s}_{i,j})$) stands for the derivation operators along $C_j^{(2)}$ (resp. $C_i^{(1)}$).

In the sequel, we assume that either one of the two sets of circles is symmetric respectively to the great circle marked with a thick line in Fig. 1, so that the point P is actually the center of the panel. In the next section we show how the right-hand-side of (2) can be evaluated with 4th order accuracy.

2.2. Definition of the Cubed-Sphere. Based on Section 2.1, the specific design of the Cubed-Sphere is obtained as follows. First we need to introduce the (ξ, η) coordinate system associated to the central circles in the panel. It is defined as follows.

- The $\xi = 0$ and $\eta = 0$ curves are orthogonal great circles (shown with a thick lines in Fig. 1). They are referred to as the η - and the ξ - equators respectively. They correspond to the circles $C_0^{(1)}$ and $C_0^{(2)}$ respectively.
- The angles ξ is the geodesic angle α along the circle $C_0^{(2)}$ and the angle η is the geodesic angle β along the circle $C_0^{(1)}$.
- The coordinate value (ξ, η) of a given point \mathbf{s} in a panel is therefore obtained by taking the two great circles at \mathbf{s} intersecting orthogonally the η - and ξ - equators respectively. Therefore ξ and η correspond to angular measures along the ξ - and η - equators.
- The full panel \mathcal{P} is defined by the two inequalities

$$(3) \quad -\frac{\pi}{4} \leq \xi, \eta \leq \frac{\pi}{4}.$$

- The grid points $\mathbf{s}_{i,j}$ on panel \mathcal{P} are defined as the points with coordinates (ξ_i, η_j) given by

$$(4) \quad \xi_i = i\Delta\xi, \quad \eta_j = j\Delta\eta, \quad -N/2 \leq i, j \leq N/2, \quad (N \text{ is supposed even}).$$

In the sequel M is the integer defined by $M := N/2$.

- Equal spacing $\Delta\xi$ and $\Delta\eta$ expresses equal geodesic distance along the ξ - and η - equators of the panel, see Fig. 5 (Left).

Due to the fact that the length of a great circle is 2π in, say, the ξ - direction, there is exactly space to insert *four* non-intersecting panels along the *East-West* direction. These four panels are called $\mathcal{P}_{I,\xi}$, $\mathcal{P}_{II,\xi}$, $\mathcal{P}_{III,\xi}$ and $\mathcal{P}_{IV,\xi}$. Similarly in the η direction (*South-North*) the four panels are called $\mathcal{P}_{I,\eta}$, $\mathcal{P}_{II,\eta}$, $\mathcal{P}_{III,\eta}$, $\mathcal{P}_{IV,\eta}$. These two series of four panels clearly overlap: a simple geometric analysis shows that we have the identities

$$(5) \quad \mathcal{P}_{I,\xi} = \mathcal{P}_{I,\eta}, \quad \mathcal{P}_{III,\xi} = \mathcal{P}_{III,\eta}.$$

This allows to define the *Cubed-Sphere grid*:

Definition 2.1 (Cubed-Sphere grid). The Cubed Sphere is the grid of the sphere \mathbb{S}^2 defined as follows: it consists of the partitionning of \mathbb{S}^2 into six identical panels referred as *Front (I)*, *East (II)*,

Back (III), West (IV), North (V) and South (VI). Each panel is equipped with its own coordinate system

$$(6) \quad (\xi^{(k)}, \eta^{(k)}), \quad -\frac{\pi}{4} \leq \xi^{(k)}, \eta^{(k)} \leq \frac{\pi}{4}, \quad (I) \leq (k) \leq (VI).$$

The points of the Cubed-Sphere are called $\mathbf{s}_{i,j}^{(k)}$. They have coordinates $(\xi_i^{(k)}, \eta_j^{(k)})$ with

$$(7) \quad \xi_i^{(k)} = i\Delta\xi, \eta_j = j\Delta\eta, \quad -M \leq i, j \leq M, \quad (I) \leq (k) \leq (VI),$$

where the step sizes are

$$(8) \quad \Delta\xi = \frac{\pi}{2N}, \quad \Delta\eta = \frac{\pi}{2N}.$$

On Panel (k) , the points $\mathbf{s}_{i,j}^{(k)}$ are classified in three categories:

(1) *Internal points*: The $(N-1)^2$ internal points $\mathbf{s}_{i,j}^{(k)}$ correspond to the indices

$$-M+1 \leq i, j \leq M-1, \quad (\text{circles on Fig 2}).$$

(2) *Edge points*: The $4(N-1)$ edge points $\mathbf{s}_{i,j}^{(k)}$ correspond to

$$j = \pm M, -M+1 \leq i \leq M-1, \quad \text{and} \quad i = \pm M, -M+1 \leq j \leq M-1, \quad (\text{squares on Fig. 2}).$$

(3) *Corner points*: The four corner points $\mathbf{s}_{i,j}^{(k)}$ correspond to

$$i = \pm M, j = \pm M, \quad (\text{pentagons on Fig. 2}).$$

Summing up the number of points $\mathbf{s}_{i,j}^{(k)}$ of each panels shows that the size of a gridfunction is $6N^2+2$.

Remark 2.2. The step size is the same on each of the six panels. The six panels are thus fully isometric and the only discrete parameter is the integer N , which stands for the number of intervals in the ξ (or η) direction of a panel.

Remark 2.3. Considering $\mathbb{S}^2 \subset \mathbb{R}^3$ as the subset of points (x, y, z) such that $x^2 + y^2 + z^2 = 1$. The relation between the coordinate (x, y, z) and the panel coordinate (ξ, η) is facilitated by the so-called *gnomonic* coordinates (53, 54). Consider for example Panel (I). The gnomonic coordinate (Y, Z) is shown in the right picture in Fig.5: they are the projection on the cube face at $x = 1$ of the coordinate $(\xi^{(1)}, \eta^{(1)})$. Observe that the grid of the face of the cube is not equally spaced in the (Y, Z) system. (We are not in any way using this grid in the sequel for calculating approximate differential operators).

3. HERMITIAN DERIVATIVE ON THE CUBED SPHERE

In this section we briefly recall the method for approximating the tangential gradient to the sphere \mathbb{S}^2 as introduced in [7]. According to (2) the gradient at point $\mathbf{s}_{i,j}^{(k)}$ is expressed in intrinsic form as

$$(9) \quad \nabla_T u(\mathbf{s}_{i,j}^{(k)}) = \frac{\partial u}{\partial \alpha}(\mathbf{s}_{i,j}^{(k)}) \mathbf{e}^\alpha(\mathbf{s}_{i,j}^{(k)}) + \frac{\partial u}{\partial \beta}(\mathbf{s}_{i,j}^{(k)}) \mathbf{e}^\beta(\mathbf{s}_{i,j}^{(k)}).$$

The great circle $C_i^{(1)}$ (resp. $C_j^{(2)}$) corresponds to an iso- ξ line (resp. iso- η line). The main idea is now to approximate the two partial derivatives $\frac{\partial u}{\partial \alpha}$ and $\frac{\partial u}{\partial \beta}$ by discrete Hermitian derivatives as

$$(10) \quad \begin{cases} \frac{\partial u}{\partial \alpha} \simeq u_{\alpha,i,j}^{(k)}, \\ \frac{\partial u}{\partial \beta} \simeq u_{\beta,i,j}^{(k)}. \end{cases}$$

This approximation follows along the lines of Hermitian discrete derivative on irregular periodic grid, as recalled in Section 7.3. The approximate tangential gradient at point $\mathbf{s}_{i,j}^{(k)}$ is given by

$$(11) \quad \nabla_{T,h} u_{i,j}^{(k)} = u_{\alpha,i,j}^{(k)} \mathbf{e}^\alpha(\mathbf{s}_{i,j}^{(k)}) + u_{\beta,i,j}^{(k)} \mathbf{e}^\beta(\mathbf{s}_{i,j}^{(k)}).$$

Consider now the $(\xi^{(k)}, \eta^{(k)})$ coordinate system. The basis $(\mathbf{g}_{\xi,i,j}^{(k)}, \mathbf{g}_{\eta,i,j}^{(k)})$, is defined by (see (59)),

$$(12) \quad \mathbf{g}_{\xi,i,j}^{(k)} = \mathbf{g}_\xi(\mathbf{x}_{i,j}^{(k)}), \quad \mathbf{g}_{\eta,i,j}^{(k)} = \mathbf{g}_\eta(\mathbf{x}_{i,j}^{(k)}).$$

This basis is related to $(\mathbf{e}_\alpha(\mathbf{s}_{i,j}^{(k)}), \mathbf{e}_\beta(\mathbf{s}_{i,j}^{(k)}))$ by the relations:

$$(13) \quad \begin{cases} \mathbf{g}_{\xi,i,j}^{(k)} = \mathbf{e}_\alpha(\mathbf{s}_{i,j}^{(k)}) \frac{\partial \alpha}{\partial \xi} |_\eta (\mathbf{s}_{i,j}^{(k)}) \\ \mathbf{g}_{\eta,i,j}^{(k)} = \mathbf{e}_\beta(\mathbf{s}_{i,j}^{(k)}) \frac{\partial \beta}{\partial \eta} |_\xi (\mathbf{s}_{i,j}^{(k)}) \end{cases} \quad -M \leq i, j \leq M, \quad (I) \leq (k) \leq (VI).$$

In (13) the functions $\xi \mapsto \alpha(\xi)$ and $\eta \mapsto \beta(\eta)$ are given in (56-58). The dual basis $(\mathbf{g}^\xi, \mathbf{g}^\eta)$ associated to the basis $(\mathbf{g}_\xi, \mathbf{g}_\eta)$ satisfies

$$(14) \quad \begin{cases} \mathbf{e}^\alpha(\mathbf{s}_{i,j}^{(k)}) = \frac{\partial \alpha}{\partial \xi}(\mathbf{s}_{i,j}^{(k)}) \mathbf{g}_{i,j}^{\xi,(k)} \\ \mathbf{e}^\beta(\mathbf{s}_{i,j}^{(k)}) = \frac{\partial \beta}{\partial \eta}(\mathbf{s}_{i,j}^{(k)}) \mathbf{g}_{i,j}^{\eta,(k)} \end{cases} \quad -M \leq i, j \leq M, \quad (I) \leq (k) \leq (VI).$$

The approximated tangential gradient is therefore expressed in the basis $(\mathbf{g}_{i,j}^{\xi,(k)}, \mathbf{g}_{i,j}^{\eta,(k)})$ by

$$(15) \quad \begin{aligned} \nabla_{T,h} u_{i,j}^{(k)} &= u_{\alpha,i,j}^{(k)} \left(\cos \eta_j \frac{1 + \tan^2 \xi_i}{1 + \cos^2 \eta_j \tan^2 \xi_i} \right) \mathbf{g}_{i,j}^{\xi,(k)} \\ &+ u_{\beta,i,j}^{(k)} \left(\cos \xi_i \frac{1 + \tan^2 \eta_j}{1 + \cos^2 \xi_i \tan^2 \eta_j} \right) \mathbf{g}_{i,j}^{\eta,(k)}. \end{aligned}$$

Referred to [7] for more details and for numerical results showing evidence of fourth-order accuracy of the approximation (15).

4. SPHERICAL DIVERGENCE

4.1. Principle of calculation. Let \mathbf{F} be a vector field tangent to the sphere \mathbb{S}^2 . The spherical divergence is expressed in the (ξ, η) coordinate system as (see Section 7.2):

$$(16) \quad \operatorname{div}_T \mathbf{F} = \frac{1}{\sqrt{G}} \left[\underbrace{\frac{\partial}{\partial \xi} (\sqrt{G} \mathbf{F} \cdot \mathbf{g}^\xi)}_{(A)} + \underbrace{\frac{\partial}{\partial \eta} (\sqrt{G} \mathbf{F} \cdot \mathbf{g}^\eta)}_{(B)} \right].$$

First consider the term (A) at a gridpoint (ξ_{i_0}, η_{j_0}) of, say, Panel (I). According to Section 2.2, we know that the iso-coordinate line $\eta = \eta_{j_0}$ is a section the circle $C_{j_0}^{(2)}$. The geodesic angle along this great circle is called $\alpha \in [0, 2\pi[$. The term (A) is calculated using the change of variable

$$(17) \quad \xi \in [-\pi/4, \pi/4] \mapsto \alpha(\xi, \eta_{j_0}).$$

where ξ is the geodesic angle along the ξ - equator (called $C_0^{(2)}$ on Fig. 1). According to the chain rule, the term (A) can be expressed as

$$(18) \quad \frac{\partial}{\partial \xi} (\sqrt{G} \mathbf{F} \cdot \mathbf{g}^\xi)(\xi, \eta_{j_0}) = \underbrace{\frac{\partial}{\partial \alpha} (\sqrt{G} \mathbf{F} \cdot \mathbf{g}^\xi)|_{\eta=\eta_{j_0}}}_{(A_1)} \underbrace{\frac{\partial \alpha}{\partial \xi}(\xi, \eta_{j_0})}_{(A_2)}.$$

The term (A_2) is a metric quantity at point $\mathbf{s}(\xi, \eta_{j_0})$ calculated once and for all (see Appendix 7).

Next we calculate an approximation of the term (A_1) using the periodic Hermitian formula (72). For that, we begin with extending the function $\xi \mapsto f^{I_\alpha}(\xi)$:

$$(19) \quad f^{I_\alpha} : \xi \in [-\pi/4, \pi/4] \mapsto (\sqrt{G} \mathbf{F} \cdot \mathbf{g}^\xi)(\xi, \eta_{j_0})$$

to the full great circle as follows. The vector \mathbf{g}^ξ at point \mathbf{s} is analytically given on Panels (I) and (III) in terms of the Cartesian coordinate $\mathbf{x}(x, y, z)$ of \mathbf{s} by, (see (61),

$$(20) \quad \mathbf{g}^\xi(\mathbf{x}) = \frac{1}{1 + \frac{y^2}{|x|^2}} \begin{bmatrix} -\frac{y}{x^2} \\ \frac{1}{x} \\ 0 \end{bmatrix}.$$

Therefore the function f^{I_α} is well defined on the two sections of great circle located on Panels (I) and (III). However due to the term $1/x$ the function $\mathbf{x} \mapsto \mathbf{g}^\xi(\mathbf{x})$ becomes singular on Panels (II) and (IV). In order to extend the function $\mathbf{x} \mapsto \mathbf{g}^\xi(\mathbf{x})$ to Panels (II) and (IV), the following vector function $\mathbf{x} \mapsto \tilde{\mathbf{g}}^\xi(\mathbf{x})$ is introduced:

$$(21) \quad \tilde{\mathbf{g}}^\xi(\mathbf{x}) = \frac{1}{1 + (y\psi(x))^2} \begin{bmatrix} -y\varphi(x)^2 \\ \varphi(x) \\ 0 \end{bmatrix}.$$

In (21) the function $x \in [-1, 1] \mapsto \varphi(x)$, (resp. $x \in [-1, 1] \mapsto \psi(x)$) are regular extensions to $[-1, 1]$ of the functions $x \mapsto 1/x$ (resp. $x \mapsto 1/|x|$). Examples of C^2 extensions using polynomials include

$$(22) \quad \varphi(x) = \begin{cases} \frac{1}{x}, & |x| \geq \frac{1}{2}, \\ 12x - 48x^2 + 64x^4, & |x| \leq \frac{1}{2}. \end{cases}$$

$$(23) \quad \psi(x) = \begin{cases} \frac{1}{|x|}, & |x| \geq \frac{1}{2}, \\ \frac{15}{4} - |x|^2 + 12|x|^4, & |x| \leq \frac{1}{2}. \end{cases}$$

In a similar fashion the metric term \sqrt{G} (see (60)) is

$$(24) \quad \sqrt{G} = r^2 \frac{(1 + X^2)(1 + Y^2)}{(1 + X^2 + Y^2)^{3/2}}, \quad (r \text{ is the radius of the sphere}).$$

It is expressed in terms of the values X and Y given on Panels (I) and (III) by

$$(25) \quad X = \frac{y}{x}, \quad Y = \frac{z}{|x|}.$$

A smooth extension to Panels (II) and (IV) is given by

$$(26) \quad \tilde{X} = y\varphi(x), \quad \tilde{Y} = z\psi(x).$$

This results in the following extension of \sqrt{G} :

$$(27) \quad \sqrt{G} = r^2 \frac{(1 + \tilde{X}^2)(1 + \tilde{Y}^2)}{(1 + \tilde{X}^2 + \tilde{Y}^2)^{3/2}}.$$

The extended function $\alpha \in [0, 2\pi[\mapsto \tilde{f}^{I_\alpha}(\alpha)$ is now defined on the full great circle:

$$(28) \quad \tilde{f}^{I_\alpha}(\alpha) : \alpha \in [0, 2\pi[\mapsto \sqrt{G} \mathbf{F} \cdot \tilde{\mathbf{g}}^\xi.$$

This function is regular on Panels (I), (II), (III) and (IV), and matches with C^2 regularity the function f^{I_α} which is defined only on Panels (I) and (III). Therefore we have

$$(29) \quad \frac{\partial}{\partial \xi} f^{(I_\alpha)}(\xi, \eta_{j_0}) = \frac{\partial}{\partial \xi} \tilde{f}^{(I_\alpha)}(\xi, \eta_{j_0})$$

$$(30) \quad = \frac{\partial}{\partial \alpha} \tilde{f}^{(I_\alpha)}(\xi, \eta_{j_0}) \frac{\partial \alpha}{\partial \xi} \Big|_{\eta=\eta_{j_0}}.$$

We can thus apply the periodic Hermitian compact operator given in (72) which provides the approximation

$$(31) \quad \frac{\partial f^{I_\alpha}}{\partial \alpha}(\xi_{i_0}, \eta_{j_0}) \simeq \tilde{f}_{\alpha, i_0, j_0}^{I_\alpha}.$$

The analog procedure in the direction η of Panel (I) gives

$$(32) \quad \frac{\partial}{\partial \eta}(\sqrt{\tilde{G}} \mathbf{F} \cdot \tilde{\mathbf{g}}^\eta)|_{\xi=\xi_{i_0}} = \frac{\partial}{\partial \beta}(\sqrt{\tilde{G}} \mathbf{F} \cdot \tilde{\mathbf{g}}^\eta)|_{\xi=\xi_{i_0}} \frac{\partial \beta}{\partial \eta}|_{\xi=\xi_{i_0}}.$$

The final discrete formula for the spherical divergence at all point $\mathbf{x}_{i,j}$ in Panel (I) is:

$$(33) \quad \operatorname{div}_{T,h} \mathbf{F}_{i,j}^{(I)} := \frac{1}{\sqrt{\tilde{G}_{i,j}}} \left(\tilde{f}_{\alpha, i, j}^{I_\alpha} \frac{\partial \alpha}{\partial \xi}(\xi_i, \eta_j) + \tilde{f}_{\beta, i, j}^{I_\beta} \frac{\partial \beta}{\partial \eta}(\xi_i, \eta_j) \right), \quad -M \leq i, j \leq M,$$

with the metric terms $\frac{\partial \alpha}{\partial \xi}(\xi, \eta)$ and $\frac{\partial \beta}{\partial \eta}(\xi, \eta)$ given in (58). Importantly, Formula (33) also holds for Panel (III) and therefore the approximate divergence on Panel (III) is an output of the same calculation as the one for Panel (I). An analogous procedure is performed for the two other couples of panels: (II)/(IV) (East-West panels) and (V)/(VI) (North-South panels).

4.2. Further comments.

4.2.1. Interpolation procedure. The calculation (33) requires a grid along the great circle on which the function \tilde{f}^{I_α} is considered. This grid is shown on Fig. 6. It consists of four sections. First the two sections on Panels (I) and (III), where the points coincide with the gridpoints having coordinates (ξ_i, η_{j_0}) . Second on Panels (II) and (IV) the points are the intercepts of the circle $C_{j_0}^{(2)}$ with the iso- ξ lines on these panels (the meridional segments, which are vertical on Fig. 6). An interpolation is performed along each of these lines to assign values to these points. Numerical evidence has shown that a cubic spline interpolation along each of these lines provides sufficient accuracy. Recall that only Hermitian derivative components in Panels (I) and (III) are finally retained. Referred to [7] for more details.

4.2.2. Computational cost. The extension of the function f^{I_α} to a regular function defined on the full great circle serves to apply the Hermitian derivative operator (72) in the periodic setting. This results in solving a tridiagonal (periodic) system of size $4N$ (71). The total cost of these resolutions is $O(N^2)$.

4.2.3. Redundancy. After solving the tridiagonal systems (72), only half of the components of the vector $f_\alpha^{I_\alpha} \in \mathbb{R}^{4N}$ is kept, namely the components located in Panels (I) and (III). The second half of the components, located in Panels (II) and (IV), is discarded. This procedure may appear costly since it has to be repeated six times (see Section 7.3 where the same principle is applied for calculating the spherical gradient) but its goal is to avoid any specific inter-panel artificial boundary treatment with e.g. ghostpoints [23]. As a consequence any alternative Hermitian (or spectral) differential approximations can be easily implemented: the periodic setting remains the same and there is no need to consider any specific interpanel treatment. It seems however possible to introduce a more clever periodic interpolation method resulting in tridiagonal linear systems of size smaller than $4N$ and retaining the same accuracy.

Further algorithmic and mathematical analysis of this interpolation procedure is postponed to future studies.

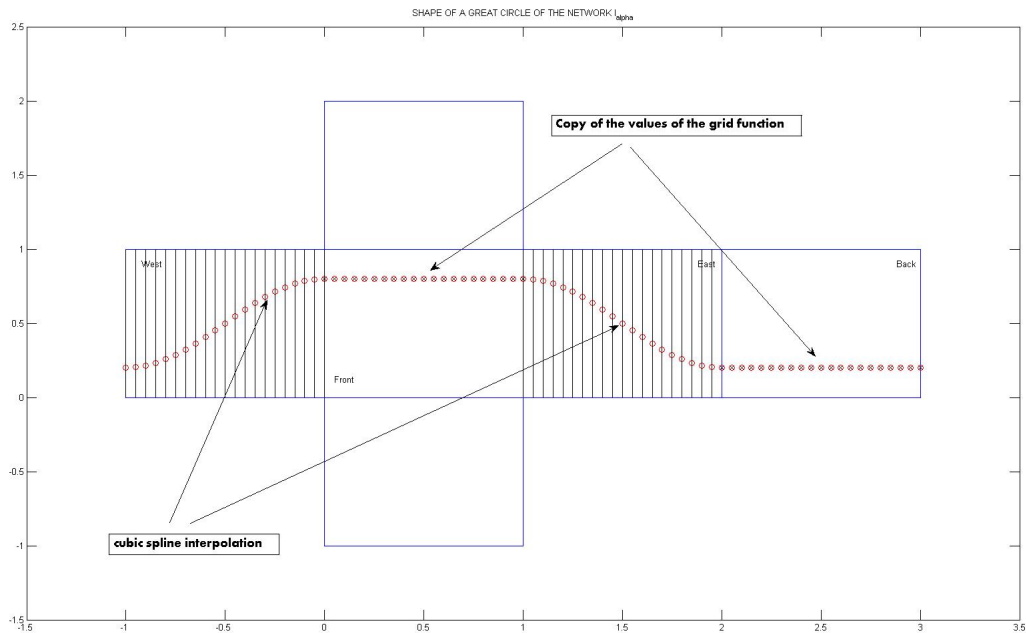


FIGURE 6. A typical coordinate great circle used in (19). The data on the great circle consist of four parts: they are simply transferred from the gridfunction data on Panels Front(I) and Back(III). On Panels East(II) and West(IV) they are deduced from the gridfunction data using cubic spline interpolation performed along the iso- ξ lines (meridian like) lines. Hermitian derivative formula (72) is then applied to these data

4.2.4. *Alternative fomulas.* Many formulas of differential geometry can be considered to calculate the spherical divergence. Instead of (16), we could have considered for example, [24]

$$(34) \quad \operatorname{div}_T \mathbf{F} = \mathbf{g}^\xi \cdot \frac{\partial \mathbf{F}}{\partial \xi} + \mathbf{g}^\eta \cdot \frac{\partial \mathbf{F}}{\partial \eta}.$$

To select a suitable formula, computational effort and efficiency have to be balanced. Formula (34) clearly requires twice more computational efforts than (33) since four Hermitian derivatives must be evaluated (two derivatives for $\frac{\partial \mathbf{F}}{\partial \xi}$ and two again for $\frac{\partial \mathbf{F}}{\partial \eta}$.)

5. NUMERICAL RESULTS

5.1. **Accuracy of the approximate spherical divergence.** The numerical accuracy of our approximate divergence (33) is evaluated using the calculated divergence of several tangential vector fields $\mathbf{x} \in \mathbb{S}^2 \mapsto \mathbf{F}(\mathbf{x}) \in \mathbb{R}^3$ of the form:

$$(35) \quad \mathbf{F}(\mathbf{x}) = \mathbf{n}(\mathbf{x}) \times \boldsymbol{\varphi}(\mathbf{x}),$$

where $\mathbf{n}(\mathbf{x})$ is the normal to the sphere and $\boldsymbol{\varphi}(\mathbf{x})$ is some vector function. In Tables 1 and 2 we report accuracy results on some examples of the so-called *geometry compatible* [2] vector fields \mathbf{F} (i.e. such that $\operatorname{div}_T \mathbf{F}(\mathbf{x}) = 0$) of the form (35). A specific example of such a vector field is given by

$$(36) \quad \boldsymbol{\varphi}(\mathbf{x}) = \nabla_T h(\mathbf{x}),$$

where $\mathbf{x} \in \mathbb{R}^3 \mapsto h(\mathbf{x})$ is a scalar function. Table 1 considers the case of a slowly varying function $h(\mathbf{x}) = \exp(x_1) + \exp(x_2) + \exp(x_3)$ with corresponding vector field

$$(37) \quad \mathbf{F}(\mathbf{x}) = \mathbf{n}(\mathbf{x}) \times \begin{bmatrix} \exp(x_1) \\ \exp(x_2) \\ \exp(x_3) \end{bmatrix}.$$

In Table 2 the same results for the oscillating function $h(\mathbf{x}) = \sin(2\pi x_1) + \sin(6\pi x_2) + \sin(10\pi x_3)$ are reported. In this case, the vector field $\mathbf{F}(\mathbf{x})$ in (37) is

$$(38) \quad \mathbf{F}(\mathbf{x}) = \mathbf{n}(\mathbf{x}) \times \begin{bmatrix} 2 \cos(2\pi x_1) \\ 6 \cos(6\pi x_2) \\ 10 \cos(10\pi x_3) \end{bmatrix}.$$

The numerical results show fourth-order accuracy between the calculated and the exact divergence (which is 0 in this case). Note that $N = 16$ corresponds to an underresolved grid.

	N=16	rate	N=32	rate	N=64	rate	N=128	rate	N=256
e_∞	9.9693(-4)	5.53	2.1537(-5)	4.79	7.7587(-7)	3.89	5.2191(-8)	3.94	3.3952(-9)
$\Delta\xi$ in km	625		312.5		156.25		78.12		39.06
Nb of grid points	1538		6146		24578		93306		393218

TABLE 1. Maximum error between the calculated and the spherical divergence for the vector field $\mathbf{F}(\mathbf{x}) = \mathbf{n}(\mathbf{x}) \times \nabla_T h(\mathbf{x})$ with $h(\mathbf{x}) = \exp(x_1) + \exp(x_2) + \exp(x_3)$, where $\mathbf{x} = (x_1, x_2, x_3)$. The exact divergence is 0. The reported error is $e_\infty = \max_{(I) \leq k \leq (VI), -M \leq i, j \leq M} |\operatorname{div}_{h,s} \mathbf{F}(\mathbf{x}_{i,j}^k)|$. The values of $\Delta\xi$ along the terrestrial equator and the total number of points are also given.

	N=16	rate	N=32	rate	N=64	rate	N=128	rate	N=256
e_∞	1.1565(2)	4.46	5.2249(0)	4.13	2.9693(-1)	4.01	1.8465(-2)	4.00	1.1558(-3)
$\Delta\xi$ in km	625		312.5		156.25		78.12		39.06
Nb of grid points	1538		6146		24578		93306		393218

TABLE 2. Maximum error between the calculated and the spherical divergence for the vector field $\mathbf{F}(\mathbf{x}) = \mathbf{n}(\mathbf{x}) \times \nabla_T h(\mathbf{x})$ with $h(\mathbf{x}) = \sin(2\pi x_1) + \sin(6\pi x_2) + \sin(10\pi x_3)$, where $\mathbf{x} = (x_1, x_2, x_3)$. The exact divergence is 0. The reported error is $e_\infty = \max_{(I) \leq k \leq (VI), -M \leq i, j \leq M} |\operatorname{div}_{T,h} \mathbf{F}(\mathbf{x}_{i,j}^k)|$. The values of $\Delta\xi$ along the terrestrial equator and the total number of points are also given.

In the third test we consider $\varphi(\mathbf{x}) = c(\mathbf{x})\boldsymbol{\psi}$ in (35) where $\boldsymbol{\psi} \in \mathbb{R}^3$ is a constant vector. Table 3 reports results for $c(\mathbf{x}) = \exp(x_1) + \exp(x_2) + \exp(x_3)$ and Table 4 for the oscillating function $c(\mathbf{x}) = \sin(2\pi x) + \sin(6\pi y) + \sin(10\pi z)$. In both cases we take $\boldsymbol{\psi} = [1, 1, 1]^T$. The vector field is

$$(39) \quad \mathbf{F}(\mathbf{x}) = c(\mathbf{x})(\mathbf{n}(\mathbf{x}) \times \boldsymbol{\psi}),$$

with spherical divergence

$$(40) \quad \operatorname{div}_T \mathbf{F}(\mathbf{x}) = \nabla_T c(\mathbf{x}) \cdot (\mathbf{n}(\mathbf{x}) \times \boldsymbol{\psi}).$$

Again a fourth-order accuracy can be observed in both cases.

	N=16	rate	N=32	rate	N=64	rate	N=128	rate	N=256
e_∞	3.2393(-3)	5.42	7.5365(-5)	4.71	2.8732(-6)	3.78	2.0855(-7)	3.94	1.3516(-8)
$\Delta\xi$ in km	625		312.5		156.25		78.12		39.06
Nb of grid points	1538		6146		24578		93306		393218

TABLE 3. Error between the calculated and the exact spherical divergence of $\mathbf{F}(\mathbf{x}) = c(\mathbf{x})(\mathbf{n}(\mathbf{x}) \times \boldsymbol{\psi})$, with $c(\mathbf{x}) = \exp(x_1) + \exp(x_2) + \exp(x_3)$, $\boldsymbol{\psi} = [1, 1, 1]^T$. The exact divergence is $\text{div}_T \mathbf{F}(\mathbf{x}) = \nabla_T c(\mathbf{x}) \cdot (\mathbf{n}(\mathbf{x}) \times \boldsymbol{\psi})$. The reported error is $e_\infty = \max_{(I) \leq k \leq (VI) - M} \max_{-M \leq i, j \leq M} |\text{div}_T \mathbf{F}(\mathbf{x}_{i,j}^k) - \text{div}_{T,h} \mathbf{F}(\mathbf{x}_{i,j}^k)|$. The values of $\Delta\xi$ along the terrestrial equator and the total number of points are also given.

	N=16	rate	N=32	rate	N=64	rate	N=128	rate	N=256
e_∞	3.3626(1)	4.45	1.5372(0)	4.29	7.8539(-2)	4.07	4.6704(-3)	4.02	2.8817(-4)
$\Delta\xi$ in km	625		312.5		156.25		78.12		39.06
Nb of grid points	1538		6146		24578		93306		393218

TABLE 4. Error between the calculated and the exact spherical divergence of $\mathbf{F}(\mathbf{x}) = c(\mathbf{x})(\mathbf{n}(\mathbf{x}) \times \boldsymbol{\psi})$ with the oscillating function $c(\mathbf{x}) = \sin(2\pi x_1) + \sin(6\pi x_2) + \sin(10\pi x_3)$, $\boldsymbol{\psi} = [1, 1, 1]^T$. The exact divergence is $\text{div}_T(\mathbf{F}(\mathbf{x})) = \nabla_T c(\mathbf{x}) \cdot (\mathbf{n}(\mathbf{x}) \times \boldsymbol{\psi})$. The reported error is $e_\infty = \max_{(I) \leq k \leq (VI) - M} \max_{-M \leq i, j \leq M} |\text{div}_T \mathbf{F}(\mathbf{x}_{i,j}^k) - \text{div}_{T,h} \mathbf{F}(\mathbf{x}_{i,j}^k)|$. The values of $\Delta\xi$ along the terrestrial equator and the total number of points are also given.

5.2. Laplacian of spherical harmonics. In this section the accuracy of the approximate divergence operator in (33) was measured using a numerical test on spherical harmonics. The spherical Laplacian is expressed in terms of the spherical divergence and spherical gradient as, [4]:

$$(41) \quad \Delta_T u = \text{div}_T(\nabla_T u).$$

Approximating (41) by composition of the discrete operators $\nabla_{T,h}$ (15) and $\text{div}_{T,h}$ (33) gives (see also [7]):

$$(42) \quad \Delta_{T,h} u(\mathbf{x}) = \text{div}_{T,h}(\nabla_{T,h} u_{i,j}^k).$$

The spherical harmonic with index (n, m) , $-n \leq m \leq n$, $0 \leq n$, is the function [15] defined in the standard spherical coordinates (θ, λ) :

$$(43) \quad f_n^m(\mathbf{x}) = \bar{P}_n^{|m|}(\sin \theta) e^{im\lambda}, \quad -\pi/2 \leq \theta \leq \pi/2, \quad 0 \leq \lambda < 2\pi,$$

where the function $\bar{P}_n^{|m|}(z)$ is the *associated Legendre polynomial* of order n, m . The standard normalization is [22]:

$$(44) \quad \int_{-1}^1 \bar{P}_n^{|m|}(x)^2 dx = 1.$$

Recall that the spherical harmonic $f_n^m(\mathbf{x})$ is an eigenfunction of the operator Δ_T with eigenvalue

$$(45) \quad \lambda_n = -n(n+1).$$

Thus at the continuous level we have

$$(46) \quad \Delta_T f_n^m - \lambda_n f_n^m = 0.$$

which can be easily assessed at the discrete level for evaluating the accuracy of the approximate Laplacian $\Delta_{T,h}$. Table 5 shows the maximum value of the error

$$(47) \quad e(f_n^m) = \max_{(I) \leq k \leq (VI) - M} \max_{-M \leq i, j \leq M} |(\Delta_{T,h} f_n^m)_{i,j}^k - \lambda_n (f_n^m)_{i,j}^k|,$$

for several spherical harmonics with increasing number of oscillations. The results are observed to

	N=16	rate	N=32	rate	N=64	rate	N=128	rate	N=256
$e(f_1^1)$	5.5934(-4)	5.93	9.1505(-6)	4.00	5.7031(-7)	2.85	7.900(-8)	2.92	1.0370(-8)
$e(f_2^2)$	1.9318(-2)	3.50	1.7162(-4)	2.92	2.2650(-5)	3.04	2.7450(-6)	2.57	4.6066(-7)
$e(f_8^4)$	2.5902(-1)	3.93	1.6950(-2)	3.21	1.8362(-3)	3.10	2.1321(-4)	3.06	2.5631(-5)
$e(f_{14}^9)$	7.9143(0)	4.10	4.6076(-1)	4.00	2.8678(-2)	3.43	2.6665(-3)	2.88	3.6298(-4)
$e(f_{25}^{18})$	2.5510(2)	4.16	1.4236(1)	3.96	9.1320(-1)	3.95	5.9231(-2)	3.93	3.8755(-3)

TABLE 5. Convergence rate of the Laplacian of several spherical harmonics. The reported errors are the max norm, $e(f_n^m) = \max_{(I) \leq k \leq (VI), -M \leq i, j \leq M} |\Delta_{h,s} f_n^m - \lambda_n f_n^m|$.

be an order of magnitude better than the ones reported in [7] where a different discrete Laplacian operator was used. The order of accuracy is around four (as long as the computer accuracy is not reached).

5.3. Duality between divergence and gradient. An approximate Hermitian gradient which is recalled in (15) was introduced in [7]. In this section we assess the compatibility of the gradient (15) with the approximate divergence (33) in the sense of an approximate version of the identity

$$(48) \quad \int_{\mathbb{S}^2} (\operatorname{div}_T \mathbf{F}(\mathbf{x}))v(\mathbf{x})d\sigma(\mathbf{x}) + \int_{\mathbb{S}^2} \mathbf{F}(\mathbf{x}) \cdot \nabla_T v(\mathbf{x})d\sigma = 0.$$

First a suitable discrete quadrature formula on the Cubed-Sphere is required. The design of accurate discrete quadrature formulas on the sphere is in itself a difficult numerical challenge. On this topic, we refer to the study [10] and the references therein.

Let $\mathbf{x} \in \mathbb{S}_r^2 \mapsto w(\mathbf{x})$ is a scalar function on the sphere of radius r . Let's consider the approximation of the integral

$$(49) \quad I = \int_{\mathbb{S}^2} w(\mathbf{x})d\sigma(\mathbf{x}) \simeq \tilde{I},$$

where

$$(50) \quad \tilde{I} = \sum_{k=(I)}^{(VI)} \tilde{I}^k.$$

The approximate integral on each Panel k , $(I) \leq k \leq (VI)$ is

$$(51) \quad \tilde{I}^k = r^2 \Delta \xi \Delta \eta \sum'_{i,j=-M}^M \sqrt{|\bar{G}_{i,j}^k|} w_{i,j}^k, \quad \bar{G}_{i,j}^k = \bar{G}^k(\xi_i, \eta_j).$$

In (50) the prime (\prime) indicates that

- the terms corresponding to the $4(N-1)$ interface points (9) are multiplied by $1/2$.
- the terms corresponding to the four corner indices (9) are multiplied by $1/3$.

Formula (50) was found to be fourth-order accurate. (This formula is the subject of ongoing research). In Table 6 and Table 7 we observe as expected that (48) is exact up to order 4. Note in Table 6 that a superconvergence for $\int F \cdot \nabla_T v$ occurs.

6. CONCLUSION

The present study demonstrates that it is possible to calculate with a high-order uniform accuracy the approximate divergence of any regular tangential vector field on the Cubed-Sphere. It is observed to be fourth-order accurate. Furthermore a discrete integration by part formula is numerically proved to be valid. This ensures the consistency between the approximate spherical gradient introduced in [7] and the approximate spherical divergence (33). In addition a preliminary test-case shows that a

	N=8	rate	N=16	rate	N=32	rate	N=64	rate	N=128
$\int \operatorname{div}_T Fv$	2.9844(-3)		1.6108(-5)		2.3363(-8)		-1.0036(-11)		-1.9540(-14)
$\int F \cdot \nabla_T v$	-1.9984(-15)		-3.3861(-15)		-1.0089(-14)		-1.8332(-14)		-3.8747(-14)
$\int \operatorname{div}_T Fv + \int F \cdot \nabla_T v$	2.9844(-3)	7.53	1.6108(-5)	9.43	2.3363(-8)	11.18	-1.0054(-11)	7.43	-5.8287(-14)

TABLE 6. Convergence rate for the value (48) applied to the functions $\mathbf{F}(\mathbf{x}) = c(\mathbf{x})(\mathbf{n}(x) \times \boldsymbol{\psi})$, with $c(\mathbf{x}) = \sin(\pi x_1) + \sin(2\pi x_2) + \sin(3\pi x_3)$, $\boldsymbol{\psi} = [1, 1, 1]^T$ and $v(\mathbf{x}) = \exp(x_1) + \exp(x_2) + \exp(x_3)$. A superconvergence of $\int \operatorname{div}_T Fv$ is observed: the computer accuracy is reached with a relatively coarse grid.

	N=8	rate	N=16	rate	N=32	rate	N=64	rate	N=128
$\int \operatorname{div}_T Fv$	10.1069		10.1303		10.1326		10.1328		10.1328
$\int F \cdot \nabla_T v$	-10.1336		-10.1329		-10.1328		-10.1328		-10.1328
$\int \operatorname{div}_T Fv + \int F \cdot \nabla_T v$	-2.6651(-2)	3.41	-2.5067(-3)	3.89	-1.6896(-4)	4.00	-1.0054(-5)	4.00	-6.5581(-7)

TABLE 7. Convergence rate for the value (48) applied to the functions $\mathbf{F}(\mathbf{x}) = c(\mathbf{x})(\mathbf{n}(x) \times \boldsymbol{\psi})$, with $c(\mathbf{x}) = \sin(\pi x_1) + \sin(2\pi x_2) + \sin(3\pi x_3)$, $\boldsymbol{\psi} = [1, 2, 3]^T$ and $v(\mathbf{x}) = \exp(x_1) + \exp(x_2) + \exp(x_3)$. Fourth-order accuracy is clearly observed.

discrete version of the Laplacian is obtained from the composition of the discrete divergence and of the discrete gradient. Further studies would be required to mathematically analyse the new method. Applying it to systems of PDEs on the sphere including the Shallow Water equations of climatology would be a natural sequel of this work.

7. APPENDIX: BACKGROUND ON THE CUBED-SPHERE

7.1. Coordinate systems on the Cubed-Sphere.

- *Cartesian coordinate system*

The cartesian reference frame is denoted by $(O, \mathbf{i}, \mathbf{j}, \mathbf{k})$, with origin O at the center of the sphere. The cartesian coordinate system is denoted $\mathbf{x}(x, y, z)$. The centers of the Panels $(I), (II), (III), (IV), (V), (VI)$ are located at points

$$(52) \quad F(1, 0, 0), B(-1, 0, 0), E(0, 1, 0), W(0, -1, 0), N(0, 0, 1), S(0, 0, -1),$$

respectively.

- (ξ, η) coordinate system

The coordinate system (ξ, η) on each Panel (k) , $(I) \leq (k) \leq (VI)$, is denoted by $(\xi^{(k)}, \eta^{(k)})$, ξ and η being the equatorial and meridional angles, respectively. Refer to Section 2.2 for a description.

- *The gnomonic coordinate system*

The *gnomonic coordinates* are defined by

$$(53) \quad \begin{cases} X = \tan \xi, \\ Y = \tan \eta. \end{cases}$$

Using (X, Y) facilitates the practical coding of any calculation on the Cubed-Sphere. For example, the cartesian coordinates of a grid point $\mathbf{x}(x, y, z)$ of, say, Panel *Front*(I), are given in terms of the equiangular angles (ξ, η) [23]:

$$(54) \quad \begin{cases} X = \frac{y}{x}, \\ Y = \frac{z}{x}, \\ x^2 + y^2 + z^2 = 1. \end{cases}$$

- *Hybrid coordinate system*

The coordinate systems (α, η) and (ξ, β) were used on each panel in Section 5. For example, on Panel *Front (I)*, the two systems are related by expressing the cartesian coordinates in terms of either (α, η) or (ξ, β) :

$$(55) \quad \begin{cases} x = \cos \alpha \cos \eta = \cos \beta \cos(-\xi), \\ y = \sin \alpha = -\cos(\beta) \sin(-\xi), \\ z = \cos \alpha \sin \eta = \sin \beta. \end{cases}$$

Suppose given $\bar{\eta} \in [-\pi/4, \pi/4]$ fixed and the corresponding iso- η line $\eta = \bar{\eta}$ on any of the six panels of the Cubed-Sphere. The angle $\alpha(\xi)$ corresponding to the point of equiangular coordinates $(\xi, \bar{\eta})$ is

$$(56) \quad \alpha(\xi) = \text{atan} \left(\frac{\tan \xi}{(1 + \tan^2 \bar{\eta})^{1/2}} \right).$$

Similarly the angle $\beta(\eta)$ corresponding to a point on any iso- ξ line $\xi = \bar{\xi}$ is

$$(57) \quad \beta(\eta) = \text{atan} \left(\frac{\tan \eta}{(1 + \tan^2 \bar{\xi})^{1/2}} \right).$$

Identities (56) and (57) give the two coordinate transforms $(\xi, \eta) \mapsto (\alpha, \eta)$ and $(\xi, \eta) \mapsto (\xi, \beta)$ on any panel. Using the chain rule again, it is readily verified that

$$(58) \quad \begin{cases} \frac{\partial \alpha}{\partial \xi} |_{\eta} = \cos \eta \frac{1 + \tan^2 \xi}{1 + \cos^2 \eta \tan^2 \xi}, \\ \frac{\partial \beta}{\partial \eta} |_{\xi} = \cos \xi \frac{1 + \tan^2 \eta}{1 + \cos^2 \xi \tan^2 \eta}. \end{cases}$$

These relations are used in (33).

7.2. Metric tensor on the Cubed-Sphere. Let us mention some remarks, useful to derive the metric elements on the Cubed-Sphere. If \mathbf{s} denotes a point on the sphere with Cartesian coordinate $\mathbf{x}(x, y, z)$, the basis $(g_\xi(\mathbf{x}), g_\eta(\mathbf{x}))$ is given by [19, 27]:

$$(59) \quad \mathbf{g}_\xi(\mathbf{x}) = \frac{\partial \mathbf{x}}{\partial \xi}(\mathbf{x}), \quad \mathbf{g}_\eta(\mathbf{x}) = \frac{\partial \mathbf{x}}{\partial \eta}(\mathbf{x}).$$

The metric tensor is

$$(60) \quad G = \begin{bmatrix} \mathbf{g}_\xi \cdot \mathbf{g}_\xi & \mathbf{g}_\xi \cdot \mathbf{g}_\eta \\ \mathbf{g}_\eta \cdot \mathbf{g}_\xi & \mathbf{g}_\eta \cdot \mathbf{g}_\eta \end{bmatrix}, \quad \bar{G} = |\det G|.$$

The associated dual basis $(\mathbf{g}^\xi, \mathbf{g}^\eta)$ is deduced by

$$(61) \quad \begin{cases} \mathbf{g}^\xi = G^{11} \mathbf{g}_\xi + G^{12} \mathbf{g}_\eta, \\ \mathbf{g}^\eta = G^{21} \mathbf{g}_\xi + G^{22} \mathbf{g}_\eta, \end{cases}$$

where

$$(62) \quad G^{-1} = \begin{bmatrix} G^{11} & G^{12} \\ G^{21} & G^{22} \end{bmatrix}.$$

The metric tensor is expressed in gnomonic coordinates (X, Y) , (53), as

$$(63) \quad G = \frac{r^2}{\delta^4} (1 + X^2)(1 + Y^2) \begin{bmatrix} 1 + X^2 & -XY \\ -XY & 1 + Y^2 \end{bmatrix},$$

where $\delta = \sqrt{1 + X^2 + Y^2}$. The dual basis $(\mathbf{g}^\xi, \mathbf{g}^\eta)$ is easily calculated in terms of $\mathbf{x}(x, y, z)$. For example on Panel *Front (I)* we have

$$(64) \quad \mathbf{g}^\xi = \frac{1}{x(1 + X^2)} \begin{bmatrix} -X \\ 1 \\ 0 \end{bmatrix}, \quad \mathbf{g}^\eta = \frac{1}{x(1 + Y^2)} \begin{bmatrix} -Y \\ 0 \\ 1 \end{bmatrix}.$$

Similar formulas are obtained for the five other panels.

7.3. Periodic Hermitian derivative. In the sequel we make intensive use of the so-called *three point* Hermitian derivative. For data u_j located on the grid $x_j = j\Delta x$, the approximation $u_{x,j} \simeq u'(x_j)$ is implicitly defined by the relation

$$(65) \quad \frac{1}{6}u_{x,j-1} + \frac{2}{3}u_{x,j} + \frac{1}{6}u_{x,j+1} = \frac{u_{j+1} - u_{j-1}}{2h}, \quad j \in \mathbb{Z}.$$

This approximation is fourth-order accurate and has a small truncation error: the leading term is given by

$$(66) \quad u_{t,j} = u'(t_j) - \frac{h^4}{180}u^{(5)}(t_j) + O(h^6), \quad 0 \leq j \leq N - 1.$$

Compact approximations of this kind were introduced earlier [6, 17]. Typical applications include wave propagation [26, 8, 9] and incompressible flow simulations [1, 3].

Here we use the approximate derivative (65) in the following context: suppose given a great circle $C_j^{(2)}$ (see Section 2.1) with curvilinear abscissa $\alpha \in [0, 2\pi[$. Let α_i be a periodic grid on $C_j^{(2)}$, with $0 \leq i \leq 4N$, (the size is $4N$, only to conform with the notation in the Section 2.2). The value α_i is defined by $\alpha_i = \varphi(t_i)$, where $t \in [0, 1] \mapsto \varphi(t)$, an increasing function (the parameter t stands for a dummy argument). The grid t_i is regular with $t_i = i\Delta t$, $0 \leq i \leq 4N$. Using the chain rule:

$$(67) \quad u'(\varphi(t)) = \frac{(u \circ \varphi)'(t)}{\varphi'(t)}, \quad 0 < t < 1.$$

Therefore the fourth-order approximation of $u'(\alpha_i)$ is

$$(68) \quad u'(\alpha_i) \simeq u_{\alpha,i} = \frac{(u \circ \varphi)_{t,i}}{\varphi_{t,i}}, \quad 1 \leq i \leq 4N,$$

where $(u \circ \varphi)_{t,i}$ and $\varphi_{t,i}$ stand for the Hermitian derivatives (65) at point t_i of $t \mapsto u \circ \varphi(t)$ and of $t \mapsto \varphi(t)$, respectively. Moving towards the practical calculation, we consider the periodic matrices $P, K \in \mathbb{M}_{4N}(\mathbb{R})$,

$$(69) \quad P = \begin{bmatrix} 4 & 1 & 0 & \dots & 1 \\ 1 & 4 & 1 & \dots & 0 \\ \vdots & \vdots & \vdots & \dots & \vdots \\ 0 & \dots & 1 & 4 & 1 \\ 1 & \dots & 0 & 1 & 4 \end{bmatrix}$$

and

$$(70) \quad K = \begin{bmatrix} 0 & 1 & 0 & \dots & -1 \\ -1 & 0 & 1 & \dots & 0 \\ \vdots & \vdots & \vdots & \dots & \vdots \\ 0 & \dots & -1 & 0 & 1 \\ 1 & \dots & 0 & -1 & 0 \end{bmatrix}.$$

Let $[\mathbf{u}], [\mathbf{x}] \in \mathbb{R}^N$ be the vector data corresponding to $(u_i)_{1 \leq i \leq 4N}$ and $(x_i)_{1 \leq i \leq 4N}$, respectively. Then the vectors $[\mathbf{u}_x], [\mathbf{x}_t] \in \mathbb{R}^N$ are solutions of the two linear systems

$$(71) \quad P[\mathbf{u}_t] = 3K[\mathbf{u}], \quad P[\mathbf{x}_t] = 3K[\mathbf{x}].$$

The components of the vector $[u_\alpha] \in \mathbb{R}^{4N}$ in (68) are given by

$$(72) \quad \bar{u}_{\alpha,i} = \frac{u_{t,i}}{x_{t,i}}, \quad 0 \leq i \leq 4N, \quad \bar{u}_{\alpha,i} = u'(\alpha_i) + O(h^4).$$

Acknowledgment: The author gratefully acknowledges an anonymous referee for the constructive criticisms which greatly helped to enhance the paper.

REFERENCES

- [1] M. Ben-Artzi, J-P. Croisille, and D. Fishelov. *Navier–Stokes equations in planar domains*. Imperial College Press, 2013.
- [2] M. Ben-Artzi, J. Falcovitz, and P.G. LeFloch. Hyperbolic conservation laws on the sphere. A geometry compatible finite volume scheme. *J. Comput. Phys.*, 228:5650–5668, 2009.
- [3] A. Brüger, B. Gustafsson, P. Lötstedt, and J. Nilsson. High order accurate solution of the incompressible Navier–Stokes equations. *J. Comput. Phys.*, 203:49–71, 2005.
- [4] M. P. Do Carmo. *Differential Geometry of Curves and Surfaces*. Prentice Hall, 1st edition, 1976.
- [5] S. Chevrot, R. Martin, and D. Komatitsch. Optimized discrete wavelet transforms in the cubed sphere with the lifting scheme - Implications for global finite-frequency tomography. *Geophys. J. Int.*, 191:1391–1402, 2012.
- [6] L. Collatz. *The Numerical Treatment of Differential Equations*. Springer-Verlag, 3-rd edition, 1960.
- [7] J.-P. Croisille. Hermitian compact interpolation on the Cubed-Sphere grid. *Jour. Sci. Comp.*, 57,1:193–212, 2013.
- [8] D.V. Gaitonde, J.S. Shang, and J.L. Young. Practical aspects of higher-order numerical schemes for wave propagation phenomena. *Int. J. Numer. Meth. Eng.*, 45:1849–1869, 1999.
- [9] I. Harari and E. Turkel. Accurate finite difference methods for time-harmonic wave propagation. *J. Comput. Phys.*, 119:252–270, 1995.
- [10] K. Hesse, I.H. Sloan, and R. S. Womersley. Chap. 40: Numerical Integration on the Sphere. In W. Freeden, M. Z. Nashed, and T. Sonar, editors, *Handbook of Geomathematics*. Springer, 2010.
- [11] L. Ivan, H. De Sterck, S. A. Northrup, and C. P. T. Groth. Three-dimensional MHD on cubed-sphere grids: Parallel solution-adaptive simulation framework. Number 2011-3382 in 20th CFD Conf. AIAA, 2011.
- [12] C. Jablonowski, P. Lauritzen, R. D. Nair, and M. Taylor. Idealized test cases for the dynamical cores of atmospheric general circulation models. A proposal for the NCAR ASP 2008 summer colloquium, 2008.
- [13] C. Jablonowski and D. L. Williamson. A baroclinic instability test case for atmospheric model dynamical cores. *Quart. J. Roy. Meteor. Soc.*, 132:2943–2975, 2006.
- [14] B.A. Jones, G.H. Born, and G. Beylkin. Comparisons of the cubed-sphere gravity model with the spherical harmonics. *Journal of guidance, control, and dynamics*, 33:415, sqq, 2010.
- [15] M. N. Jones. *Spherical Harmonics and Tensors for classical field theory*. Research Studies Press, 1985.
- [16] P. Lauritzen, R. D. Nair, and P. A. Ullrich. A conservative semi-Lagrangian multi-tracer transport scheme (CSLAM) on the cubed sphere grid. *J. Comput. Phys.*, 229:1401–1424, 2010.
- [17] S. K. Lele. Compact finite-difference schemes with spectral-like resolution. *J. Comput. Phys.*, 103:16–42, 1992.
- [18] R. D. Nair and P. Lauritzen. A class of deformational flow test cases for linear transport problems on the sphere. *J. Comput. Phys.*, 229:8868–8887, 2010.
- [19] R. D. Nair, S. Thomas, and R. Loft. A discontinuous Galerkin transport scheme on the cubed sphere. *Mon. Wea. Rev.*, 133:814–828, 2005.
- [20] F. Natterer and F. Wübbeling. *Mathematical methods in image reconstruction*. SIAM, 2001.
- [21] C. Jablonowski R. D. Nair. Moving vortices on the sphere: a test-case for horizontal advection problems. *Mon. Wea. Rev.*, 136:689–711, 2008.
- [22] V. Rokhlin and M. Tygert. Fast algorithms for spherical harmonic expansions. *SIAM J. Sci. Comput.*, 27:1903–1928, 2006.
- [23] C. Ronchi, R. Iacono, and P. S. Paolucci. The Cubed Sphere: A new method for the solution of partial differential equations in spherical geometry. *J. Comput. Phys.*, 124:93–114, 1996.
- [24] J. G. Simmonds. *A Brief on Tensor Analysis*. Undergraduate Texts in Math. Springer, 2cd edition, 1994.
- [25] J.-L. Starck, Y. Moudden, P. Abrial, and M. Nguyen. Wavelets, ridgelets and curvelets on the sphere. *Astronomy and Astrophysics*, 446:1191–1204, 2006.
- [26] C. K. W. Tam and J. C. Webb. Dispersion-relation-preserving finite difference schemes for computational acoustics. *J. Comput. Phys.*, 107:262–281, 1993.

- [27] P. A. Ullrich, C. Jablonowski, and B. van Leer. High order finite-volume methods for the shallow-water equations on the sphere. *J. Comput. Phys.*, 229:6104–6134, 2010.
- [28] D. L. Williamson. The evolution of dynamical cores for global atmospheric models. *J. Meteo. Soc. Japan*, 85B:241–269, 2007.

†UNIVERSITÉ DE LORRAINE, DÉPARTEMENT DE MATHÉMATIQUES, F-57045 METZ, FRANCE, ‡C.N.R.S., INSTITUT ELIE CARTAN DE LORRAINE, UMR 7502, F-57045 METZ, FRANCE

E-mail address: `jean-pierre.croisille@univ-lorraine.fr`